

Lithium Salt Effects on the Liquid Structure of Choline Chloride–Urea Deep Eutectic Solvent

Maria Enrica Di Pietro,^{*,†} Kateryna Goloviznina,[†] Adriaan van den Bruinhorst, Giselle de Araujo Lima e Souza, Margarida Costa Gomes, Agilio A. H. Padua,^{*} and Andrea Mele



Cite This: *ACS Sustainable Chem. Eng.* 2022, 10, 11835–11845



Read Online

ACCESS |



Metrics & More



Article Recommendations

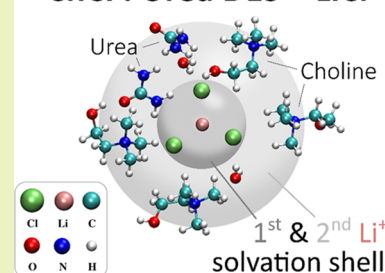


Supporting Information

ABSTRACT: Deep eutectic solvents (DESs) added with lithium salts are emerging as alternative electrolytes for lithium-ion batteries (LIBs). Yet, to design, optimize, and develop efficient DES-based electrolytes for LIBs, an in-depth understanding of the role played by the lithium cations in the intermolecular interactions between all species in the mixture is crucial. A joint approach of experimental NMR techniques and polarizable molecular dynamics (MD) simulations is used here to gather a comprehensive picture of the structure and dynamics of the prototypical system composed of the DES choline chloride:urea (ChCl:U, $x_{\text{ChCl}} = 0.33$) and the lithium salt containing the same anion, LiCl. Strong coordination of lithium cations by chloride anions, resulting in the formation of LiCl_3^{2-} units, is revealed. Other species (especially, urea) are present in the second coordination shell of lithium, creating an extensive hydrogen-bond network. The effect of small quantities of water, typically absorbed by DES from air moisture, on the studied properties is discussed.

KEYWORDS: eutectic electrolytes, molecular dynamics, nuclear magnetic resonance, lithium salt, local structure, dynamics, polarizable force field

ChCl : Urea DES + LiCl



INTRODUCTION

The global electrochemical energy storage market is currently dominated by Li-ion batteries (LIBs). LIBs are at present the best-performing rechargeable batteries and are most widely used.¹ However, the safety of LIBs is still an issue due to the thermally unstable and highly flammable electrolyte solution used.¹ Indeed, thermal, mechanical, or electrical abuse may result in an uncontrollable thermal runaway process with battery failure and possible leakage of hazardous chemicals as a consequence.^{2,3}

Although considerable efforts have been spent on the design of nonflammable liquid electrolyte systems for rechargeable LIBs, a viable electrolyte solution to replace LiPF_6 /carbonate mixtures does not exist yet. Room-temperature ionic liquids (ILs) have been presented as a safer replacement for organic electrolytes,⁴ but their wide application is still hampered by their high cost, quite complicated synthesis, potential toxicity, and hazardous environmental impact.⁵ Deep eutectic systems (DESs) are an alternative to both flammable organic solvent-based electrolytes and ILs. They are mixtures of two or more components that show marked melting point depressions and can yield low-cost and highly sustainable liquid materials at ambient temperatures.^{2,6} Choline chloride (ChCl)-based DESs are of particular interest for LIBs, showing six times higher conductivity than the LiCl-based DES with the same HBD.⁷

Large amounts of lithium salts can be dissolved in ChCl-based DESs, 2.1 mol kg^{-1} in ChCl:urea (ChCl:U) at a 1:2 molar ratio at room temperature.⁸ The physicochemical

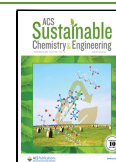
properties of DESs—the melting point depressions, in particular—generally stem from a fine balance of intermolecular interactions and liquid organization. The addition of small positively charged lithium ions will alter this balance, thus affecting the micro- and macroscopic properties. For instance, the density and viscosity of ChCl:U increase upon the addition of LiCl,⁹ slowing down the motion of the ions in the bulk liquid. Similarly, a decrease in ^1H diffusivities and a perturbation of the solvent's structural organization were observed upon the addition of lithium salts to ChCl-based DESs.^{10,11} It has to be noted that the investigated anions are of different nature than Cl, affecting the Li coordination and ion aggregation.¹⁰ To design, optimize, and develop DES-based electrolytes for LIBs, it is therefore important to gain an in-depth understanding of the intermolecular interactions between all species in the mixture and to signify the role of the Li cation.

Here, we focus on the prototypical system composed of the DES ChCl:U ($x_{\text{ChCl}} = 0.33$) and the lithium salt containing the same anion, LiCl. Using a joint approach of experimental nuclear magnetic resonance (NMR) techniques and polar-

Received: April 25, 2022

Revised: August 17, 2022

Published: August 30, 2022



izable molecular dynamics (MD) simulations based on the CL&Pol force field,^{12,13} we attempt to (i) single out the role of the newly introduced Li^+ cation in the system, (ii) elucidate the rearrangement of the intermolecular interactions between urea, choline, and chloride at the atomic to molecular level, and (iii) shed light at the impact of residual water¹⁴ on the interactions within the DES as well as the physical–chemical features of the systems.

EXPERIMENTAL SECTION

First, $\text{ChCl}:\text{U}$ $x_{\text{ChCl}} \approx 0.33$ was prepared. Subsequently, 1.6 wt % of LiCl was added. The resulting mixture had a water content of 3.9 wt % and is hereafter referred to as $\text{ChCl}:\text{U}-\text{LiCl}-\text{W}$. A detailed description of the sample preparation is given in the [Supporting Information](#). Such a small amount of water does not significantly disrupt the intermolecular interactions found in neat DESs,¹⁵ while it can mitigate some drawbacks, mainly viscosity. The sample was used for one-dimensional (1D) and two-dimensional (2D) ^1H and ^7Li NMR experiments as well as density/viscosity measurements (details are given in the [Supporting Information](#)). The same sample and its anhydrous analogue ($\text{ChCl}:\text{U}-\text{LiCl}$) were simulated using molecular dynamics with the polarizable CL&Pol force field. The force field model was validated through the comparison of the calculated equilibrium and transport properties with experimental data. Radial, angular, and spatial distribution functions (RDF, ADF, and SDF, respectively) were computed to reveal trends in the local structure. Diffusion coefficients, viscosity, and rotation correlation times were calculated to analyze the dynamics of the systems. The complete simulation procedure and the force field development methodology are described in the [SI](#).

RESULTS AND DISCUSSION

The present work aims at addressing two key questions considering $\text{ChCl}:\text{U}-\text{LiCl}$ as a prototypical DES-based electrolyte:

- How is the structure of local environments of Li^+ in the DES mixture?
- How are all other components of the system arranged in terms of structure and dynamics?

To this end, we use a joint NMR/MD approach on the same system $\text{ChCl}:\text{U}-\text{LiCl}-\text{W}$. First, the peculiar arrangement of Li^+ ions is probed experimentally by heteronuclear NOE NMR and theoretically via MD simulations. Wider insights into the whole electrolyte system are gained through MD simulations, on the one side, and temperature-dependent NMR measurements, on the other. To finally dissect the effect of water, MD simulation results of the *in silico* water-free system $\text{ChCl}:\text{U}-\text{LiCl}$ will be presented.

Focusing on Lithium Ions: Local Environment.

Proton–lithium heteronuclear Overhauser effect spectroscopy ($^1\text{H}-^7\text{Li}$ HOESY) was used to gain insights into short-range correlations around lithium cations ([Figure S1](#)), assuming that the upper limit for detecting $^1\text{H}-^7\text{Li}$ contacts is ca 5 Å. Indeed, the markedly different ^1H and ^7Li gyromagnetic ratios allow us to overcome the long-ranged nature of the intermolecular NOE, thus truly reflecting the short-range connectivities around Li^+ .^{16–18} Normalized NOE build-up curves obtained at 298 K at variable mixing times (50 ms–3 s) were fitted using a modified version of the Solomon equation for a dipolar-coupled heteronuclear system,^{19,20} with the relative cross-relaxation σ_{IS} as the only parameter ([Figures 1 and SI](#) for a theoretical description). The closest proximity is between Li^+ and urea NH_2 protons, but a consistent cross-relaxation is also observed with the *N*-trimethylammonium head of Ch. The

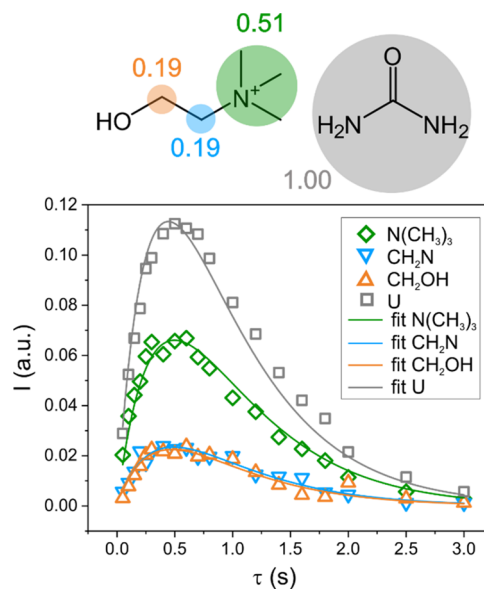


Figure 1. Normalized $^1\text{H}-^7\text{Li}$ NOE build-up curves fitted using eq S5,^{19,20} and corresponding relative cross-relaxation rates normalized to the highest value.

NOE on the methylene protons is, on the other hand, quite small. As water and choline OH protons do not give a well-resolved NMR signal, no cross-relaxation can be extracted for these protons. The anion is unfortunately missing in the NMR-derived picture of the system, albeit it is expected to play a crucial role. Actually, the data in [Figure 1](#) show a counter-intuitive finding of a positive ion (Li^+) in close spatial proximity to a formally positively charged quaternary ammonium group. The picture emerging from NOE data is then consistent with the Li^+ ions not behaving as individual moieties with a full positive charge. Rather, the molecular environment of Li^+ includes the chloride ions bound to Li^+ in its solvation shell, giving rise to the negatively charged species of type $[\text{LiCl}_n]^{(n-1)-}$.

MD simulations reveal that the strongest interaction of lithium is with the chloride anion, appearing as a high peak with a maximum at 2.32 Å, as shown in [Figure 2a](#). The peak intensity reaches 76, which is not surprising since similar probabilities were reported in the literature for lithium interacting with vinylene carbonate²¹ and with glymes.^{22,23} Formed at a distance of 3.02 Å, the first coordination shell includes 3.0 chloride anions around each lithium cation, arranged in a planar triangular LiCl_3^{2-} unit. The existence of similar negatively charged complexes with the TFSI-based, dicyanamide, tetrafluoroborate, hexafluorophosphate, nitrate, and other anions has been recently discussed.^{24–29} For instance, the presence of $[\text{Li}(\text{TFSI})_x]^{x-1-}$ units in the LiTFSI/IL solution was confirmed by Raman spectroscopy, NMR, X-ray diffraction, and *ab initio* molecular dynamics.^{29–33} Since the chloride anion is a smaller ion with a well-localized charge, when compared to bulky TFSI, the formation of lithium chloride complexes is more than expected.

The interaction of lithium with urea and cholinium protons ([Figure 2b](#)), which is observed experimentally, is indirect, through the chloride anion ([Figure 3a–d](#)), as these species are found in the second coordination shell of lithium at a characteristic distance of 5.05 Å. Although the intensity of this peak for the cholinium head group is greater than for urea, we

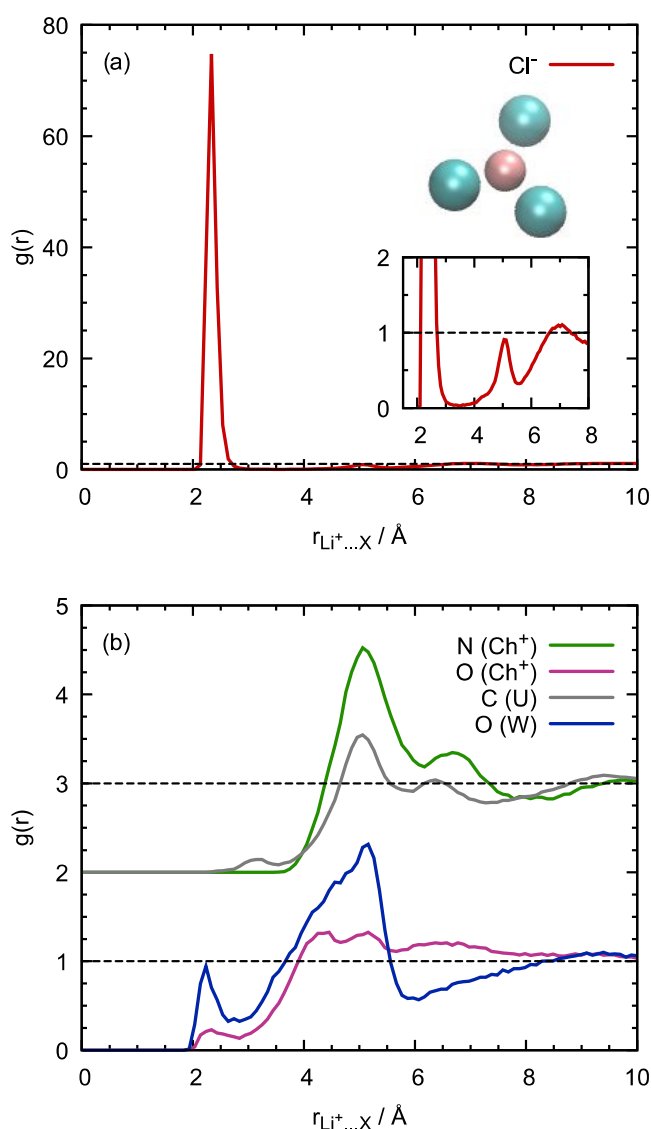


Figure 2. Radial distribution functions of selected atoms around the lithium cation in the ChCl:U–LiCl–W system with the respective vertical offsets of 0.0 and 2.0.

should be aware of a twice smaller number of cholinium ions that are taken into account when normalizing the RDFs. Indeed, urea dominates in the second coordination shell with 6.75 molecules (up to $r_{\min} = 7.32$ Å), while only 5.6 cholinium cations are found around lithium (up to $r_{\min} = 7.72$ Å). Contrary to the NOE experiments, in which the quantitative detection of hydroxyl protons is problematic, MD shows the presence of 1.65 water molecules (up to $r_{\min} = 5.92$ Å) in the close environment of lithium, whereas the interaction of the alkali metal ion with the hydroxyl group of cholinium is not marked. The coordination numbers given above include a direct interaction of lithium with the oxygen atoms of water and with urea, with a nonprominent peak appearing at 2.2 Å on $\text{Li}\cdots\text{O}_w$ RDFs and a corresponding contribution at 3.2 Å in the $\text{Li}\cdots\text{C}_U$ RDF. These interactions are overwhelmed by the interaction of chloride with the metal ion since there are 10 anions per lithium cation present in the system (Table S1).

We also observed a shift in a phase boundary between LiCl and DES–W species, occurring in sufficiently long trajectories (details given in the SI). Lithium salt appears to be much less

soluble in MD simulation than what is known from experiments, which points to limitations of our model.

Looking Wider to the Electrolyte: Structure and Dynamics. To complete the structural analysis of the system studied, we looked into the extensive hydrogen-bond network formed by the DES components and water. Chloride appears as the major H-bond acceptor, 70% of which interacts with the hydrogen atoms of cholinium, urea, and water, whereas the remainder is captured by the electrostatic attraction of lithium. The anion forms medium-strength hydrogen bonds with water and with the hydroxyl groups of cholinium, at typical distances of 2.1–2.2 Å (Figure 4a) and with a $\text{Cl}\cdots\text{H}-\text{O}$ angle of 155–180° (Figure S10). A weaker and less probable interaction is observed with hydrogen atoms of urea at 2.35 Å. The methyl and methylene hydrogens are found at 2.9 Å from chloride and show broad and flat angular distributions (Figure S10), arising from a variety of available cholinium chloride configurations, recently studied via first-principles calculations.³⁴ The first coordination shell includes 0.67 H_2O atoms from cholinium (up to $r_{\min} = 3.28$ Å), 0.85 H_w from water (up to $r_{\min} = 3.02$ Å), and 2.95 H_U from urea (up to $r_{\min} = 3.15$ Å); the peak at 3.51 Å on the RDF of the H_w of water was not included in the integration because it represents the second hydrogen atom from a water molecule and is not interacting directly with the chloride anion. The coordination numbers of hydrogen atoms around chloride are bigger than that of lithium (0.30 Li^+ around each chloride), pointing to the possible competition between these species for the anion. However, the chloride–lithium interaction remains dominant (as seen from the ratio of peak intensities in Figures 2a and 4a), and the observed coordination numbers reflect the greater molar fraction of DES/W with respect to the lithium salt in the mixture.

The oxygen atom of urea is a weaker H-bond acceptor (Figures 3c and 4b), its interaction with H_2O and H_w atoms appearing at 1.9 Å with a well-defined but low-intensity peak. Hydrogen atoms from urea and from methyl groups of cholinium show slightly higher intensities with maxima at 2.15 and 2.58 Å, respectively. Here, we do not provide the coordination numbers of selected atoms around urea since it is difficult to define the exact boundaries between the coordination shells.

Water, on the contrary, acts mainly as a H-bond donor and not an acceptor since the $\text{O}_w\cdots\text{H}$ interactions are less prominent, as shown in Figures 3d and 4c. They are found as prepeaks at 1.95 and 2.1 Å in the H_w and H_O RDFs, respectively, and no clear maximum is present in the H_U curve. In addition, the peak of the methyl hydrogen atoms at 2.75 Å is shifted to longer distances when compared to the $\text{O}_U\cdots\text{H}_1$ RDF. A dominant donor role of water can be noticed from the intense peak at 3.28 Å in the $\text{O}_w\cdots\text{H}_w$ RDF, which represents the separation between two water molecules situated in the first coordination shell of the same chloride anion. The oxygen atom of the hydroxyl group of cholinium (Figure 3a) is almost not involved in H-bond interactions with water. Similarly to urea, the coordination numbers around water are not given here.

The general trends in the DES–W structure are in agreement with the recent *ab initio*³⁵ and classical MD³⁶ studies and also with X-ray scattering experiments,³⁷ but a direct comparison is not plausible due to the different water contents considered in these studies and due to the presence of the lithium salt in our system.

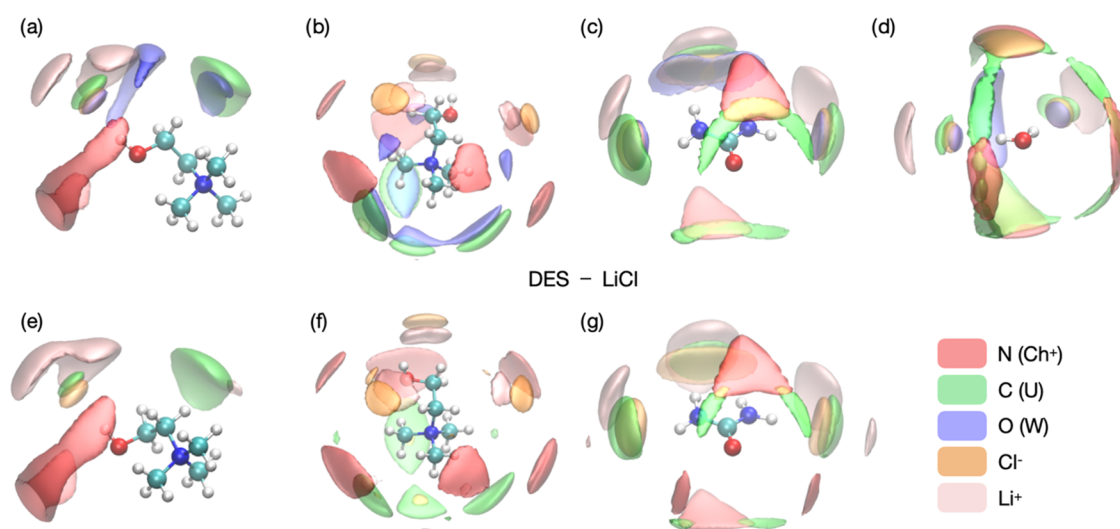


Figure 3. Spatial distribution functions of selected atoms around hydroxyl (a, e) and ammonium (b, f) groups of cholinium, urea (c, g), and water (d) in the ChCl:U-LiCl-W (top) and ChCl:U-LiCl (bottom) systems. Isodensity contours at (a, e) 5.0 N (Ch⁺), 2.7 C (U), 3.8 O (W), 60.0 Cl, 7.5 Li; (b, f) 3.0 N (Ch⁺), 3.6 C (U), 3.8 O (W), 6.5 Cl, 3.4 Li; (c, g) 6.5 N (Ch⁺), 3.6 C (U), 3.5 O (W), 12.0 Cl, 5.0 Li; and (d) 5.0 N (Ch⁺), 2.7 C (U), 4.6 O (W), 80.0 Cl, 15.0 Li times the average density around the central ion.

Even though water and choline OH protons did not give a well-resolved NMR signal, temperature-dependent NMR measurements in the range of 278–373 K were useful to unveil complementary information on the other sites/species (methyl and methylene protons of Ch, U protons, and Li). A first insight into the interaction strength experienced by the different species can be gained by following the chemical shift over temperature (Figure S2). As expected, an upfield shift is observed for all signals as a result of the weakening of the interactions due to the increase in temperature. More in detail, urea protons are the most affected ($|\delta(373\text{ K}) - \delta(278\text{ K})| = |\Delta\delta^{\text{max}}| = 0.35\text{ ppm}$), followed by lithium cations ($|\Delta\delta^{\text{max}}| = 0.19\text{ ppm}$), while choline signals are barely affected ($|\Delta\delta^{\text{max}}| = 0.04\text{ ppm}$), thus reflecting qualitatively the strength of the interactions.

Traditional dynamic NMR parameters such as diffusion coefficients and relaxation times can be exploited to indirectly get structural information on the system. Indeed, structure and dynamics are intimately related, as the translational and rotational motion of a site/species intuitively depends also on the strength of its interactions with the surroundings. Self-diffusion coefficients and T_1 relaxation times were measured over a 95 K temperature interval and analyzed to get the quantitative descriptors of the motion.

Table S4 and Figure S4a show the self-diffusion coefficients measured for the different species by PFG NMR. All cholinium protons exhibited the same diffusivity, as expected; hence, the value of CH₃ is presented. The respective self-diffusion coefficients for U, Ch, and Li are close but still different, even at the lowest temperature (at 283 K and in m²s⁻¹, 3.4×10^{-12} for U, 2.7×10^{-12} for Ch, and 1.4×10^{-12} for Li), confirming the existence of an extended intermolecular network that slows down the individual motion but at the same time the absence of stable (on the NMR time scale) contact ion pairs or aggregates. Diffusivity follows the order U > Ch > Li, which clearly does not correlate with size. Indeed, U moves faster than Ch, as expected from their molecular weights and already observed in other DESs,^{38–40} but Li is the smallest species in the mixture, yet it is also the slowest one in the whole temperature range (except at very high T). The behavior

is similar to what is typically observed for ionic liquids^{21,24,41,42} and likely stems from the strong interaction of lithium cations with chloride anions.

The polarizable MD simulations predict the dynamics well, with relative deviations between the experimental and calculated diffusion coefficients not exceeding 30%, as seen in Table 1. These positive deviations are reflected in (minor) viscosity underestimations. The simulation approach provides an access to the diffusion coefficients of water and chloride, complementing the NMR data. Thus, water is the fastest species in the system, which agrees well with its small molecular weight. The diffusivity of DES species decreases in the order U > Cl > Ch, being consistent with a previous MD study of the DES-W system by Harries³⁶ (Figure 1D of that article). Note that the presence of the lithium salt in our systems reduces significantly the diffusion coefficient of chloride, which now becomes closer to that of cholinium than that of urea. This is a result of a strong electrostatic interaction between lithium and chloride, as discussed herein.

The experimental temperature dependence of the diffusion coefficients over the whole probed temperature range was first approximated to Arrhenius behavior, yielding translational activation energy E_a^{transl} in the order: Li (44.0 kJ mol⁻¹) \approx U (43.5 kJ mol⁻¹) > Ch (39.3 kJ mol⁻¹) (Figure S4b and Table S5). However, the Arrhenius plots of the D values are slightly curved, especially for U ($R^2 = 0.990$), and would be better approximated using a relationship of the Vogel–Fulcher–Tammann (VFT) type (Table S6). Since the slopes of the plots were somewhat discontinuous around 320 K, we chose to perform a further Arrhenius analysis distinguishing two ranges, 278–318 K and 323–373 K (Figure S4a,b and Table 2). As expected, the thermal activation energy for the translational diffusion is smaller in the higher temperature range. In both ranges, E_a^{transl} of Li is ca. 7 kJ mol⁻¹ higher than E_a^{transl} of Ch. The most marked change between the two temperature intervals is observed for E_a^{transl} of U, which is closer to that of Li in the low-temperature range (51.7 vs 49.4 kJ mol⁻¹) and comparable to that of Ch in the high-temperature range (34.9 vs 35.3 kJ mol⁻¹). A somehow related behavior is found when calculating the activation energies for the fluidity (defined as

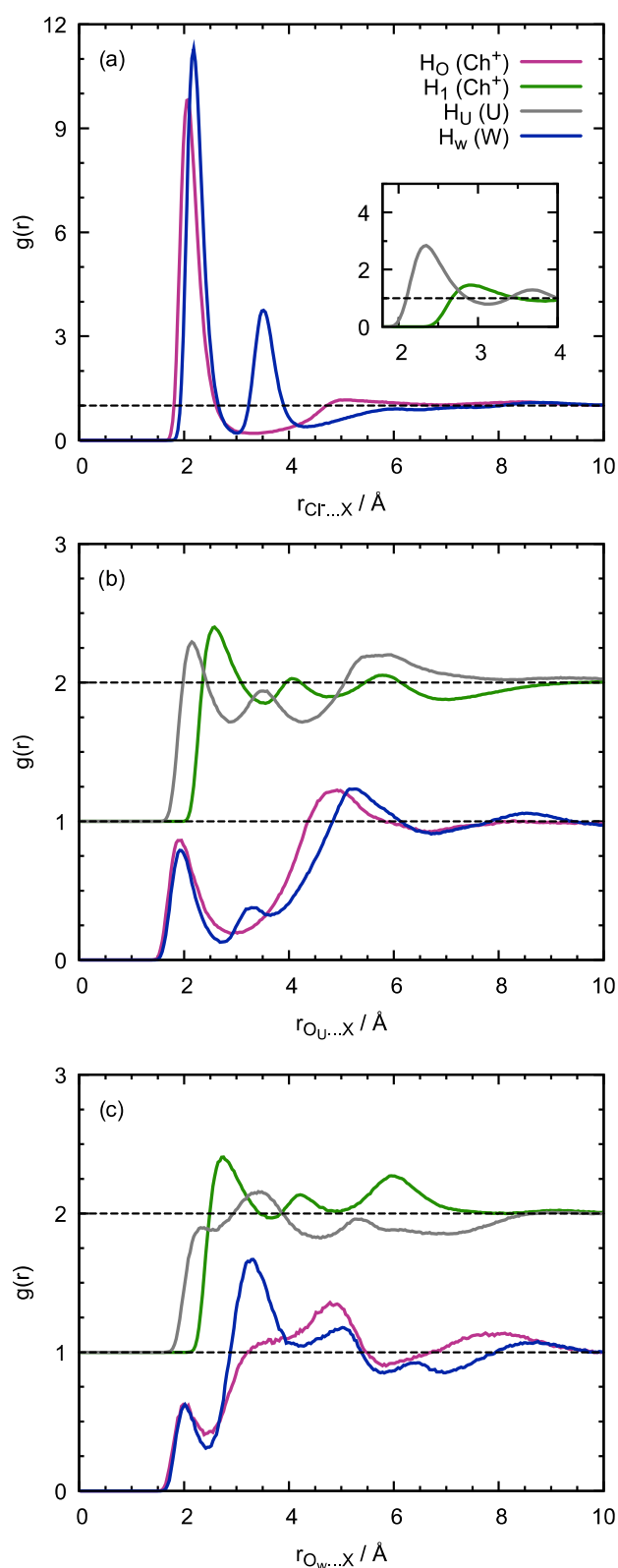


Figure 4. Radial distribution functions of selected hydrogen atoms around the chloride anion (a), around the oxygen atom of urea (b), and around the oxygen atom of water (c) in the ChCl:U–LiCl–W system. The H_O and H_1 atoms correspond to the H atoms of hydroxyl and methyl groups of cholinium, and H_U and H_w are the H atoms of urea and water, respectively. The vertical offsets in panels (b) and (c) are 0.0 and 1.0.

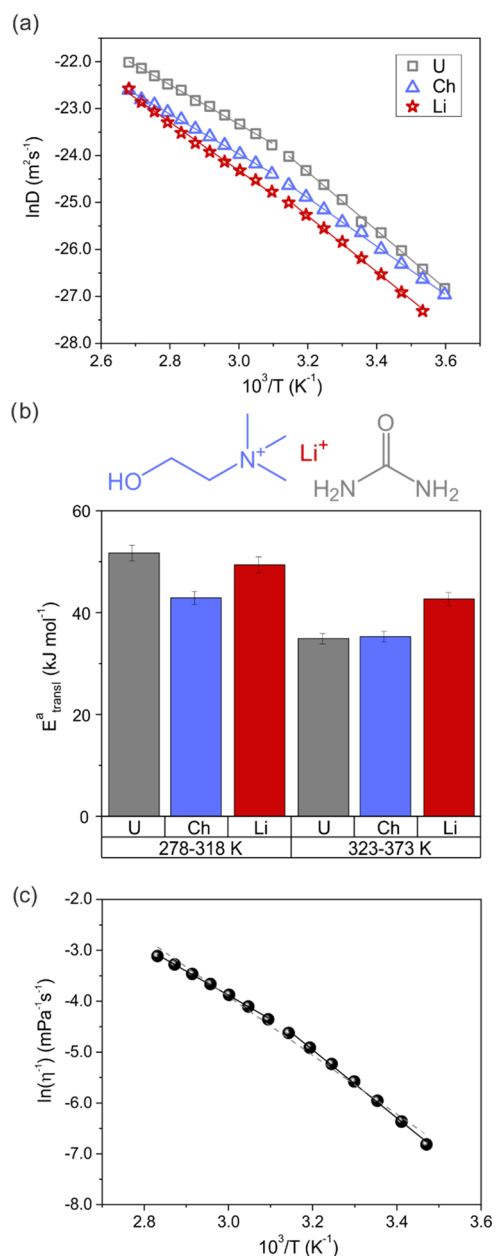
the reciprocal of the viscosity η^{-1}) from the slope of the linear regression of the Arrhenius plot (Figure 5c).⁴² Values of 55.6 and 39.3 kJ mol^{−1} were extracted when considering a low- (below 320 K) and high- (above 320 K) temperature region, respectively (Table S7). The significant difference between the two regions (16.3 kJ mol^{−1}) closely reflects that found for E_a^{transl} of urea (16.8 kJ mol^{−1}).

The picture in the high-temperature interval very much resembles that found by some of us in the *N,N*-methylbutylpyrrolidinium (PYR₁₄) TFSI ionic liquid doped with LiTFSI.⁴² In that case, the observed activation energy surplus of ca 10 kJ mol^{−1} found for Li⁺ diffusivity compared to that of both TFSI and PYR₁₄ was ascribed to a different diffusion mechanism occurring for Li⁺ diffusion, i.e., the structure–diffusion rather than the vehicular mechanism. In other words, the higher energy barrier found for Li cations stems from the complex set of steps required for the “hopping” mechanism of Li⁺ diffusion. However, in the case of the Li-doped IL, the network of interactions is simpler than that emerging from this study on the ChCl:U–LiCl–W system. Actually, when considering the components of the DES–LiCl system object of this work, the Li ions are strongly coordinated to chlorides and, at the same time, the resulting Li–Cl complexes are, in turn, strongly interacting with U, as highlighted by NOE and MD results of the previous section. Thus, having in mind the data of Table 2, in this case, the most peculiar behavior is shown by U itself, showing quite a correlated activation parameter with Li–Cl complexes in the low *T* regime and a correlated activation parameter with Ch in the high *T* regime. U plays a well-recognized major role in the DES intermolecular network, and these findings underline that the energy barrier to its transport—hence likely the strength of its H-bonds with other partners—is strongly temperature-dependent in DES–LiCl systems. The marked temperature dependence of the activation energy of urea actually emerges when the Litovitz equation is used to fit the self-diffusion coefficients (Figure S5).^{43,44} The better fit obtained for U with respect to a simple Arrhenius model (Tables S5 vs S8) can be seen as an indication that the activation energy of this species is a function of its average H-bond interactions in the system, which, in turn, change with temperature.⁴³

The combined use of diffusion and viscosity data may help shed light on the diffusion mechanism.³⁸ It is known that the diffusivity of species in DESs and ILs deviates from the Stokes–Einstein behavior,^{38,45–47} and a correlation length can instead be calculated as $\xi = kT/c\pi\eta D$ (with *k* being the Boltzmann constant, *T* being the absolute temperature, and *c* being a constant theoretically ranging between 4 and 6 for slip and stick boundary conditions, respectively).^{38,48} From Figure 6, it can be seen that ξ increases with increasing temperature for all of the three species in the studied system, and the ξ values for the choline cation in the mixture are for both *c* = 4 or 6 smaller than the ionic radius (3.29 Å).^{38,39,49} This agrees with results reported for pure ChCl:U and other DES^{38,45} and confirms a non-Stokesian diffusion, which is a relevant information in applications of DESs—and molecular liquids, in general—that involve the exploitation of charge transport rather than just their properties as solvents⁵⁰ (see also Figure S6). This deviation in DESs has been ascribed to a diffusion mechanism similar to that occurring in ILs, in which a species migrates via a series of discrete jumps between voids or holes in the liquid, and the correlation length is a measure of the size of the “space” into which the species can jump.

Table 1. Experimental (exp) and Calculated (sim) Properties of DES-Based Electrolytes at 353 K Densities (ρ) Are Given in g cm⁻³, Diffusion Coefficients (D) in 10⁻¹¹ m² s⁻¹, and Viscosities (η) in mPa s

system	ρ	$\rho^{\text{dev}}/\%$	$D(\text{Ch}^+)$	$D(\text{Cl}^-)$	$D(\text{U})$	$D(\text{Li}^+)$	$D(\text{W})$	η
ChCl:U–LiCl–W								
exp	1.1662		8.1		15.2	6.1		22.5 ± 0.2
sim	1.1402	−2.2	10.4	12.7	18.1	7.3	34.9	16 ± 2
ChCl:U–LiCl								
sim	1.1645		3.4	4.9	7.4	3.1		55 ± 28

**Figure 5.** (a) Arrhenius plots of diffusion data obtained for Ch, U, and Li over two temperature subintervals (278–318 and 323–373 K) and (b) the corresponding translational activation energy E_a^{transl} obtained from the Arrhenius plots over different temperature ranges. Fit parameters are listed in Table 2. (c) Arrhenius plot of the temperature dependence of the fluidity over the whole temperature range (288.15–353.15 K, dashed gray line) and two subintervals (288.15–318.15 and 323.15–353.15 K). Fit parameters are listed in Table S7.

To gather a more complete overview of the system, ¹H T_1 relaxation times were measured as a function of temperature (Figure 7a). All signals pass through a minimum, which is interpreted as the transition from the diffusion limit ($\omega_0\tau_C > 1$, at lower T) to the extreme narrowing ($\omega_0\tau_C < 1$, at higher T) relaxation regime. CH₂ and CH₃ groups of cholinium exhibit a minimum at ca. 295 K, U at 313 K, and Li at 323 K. Even if interpreted with care, given the contributions of different relaxation mechanisms—from intramolecular rotation to spin diffusion, which add to dipolar interactions, as well as quadrupolar relaxation for Li—this qualitatively indicates that faster local dynamics occurs for Ch protons when compared to U and Li.

The spin–lattice T -dependent relaxation data were quantitatively analyzed using the Bloembergen, Purcell, and Pound (BPP) model^{40,41,51–53} to get the correlation time τ_C and the apparent activation energy for the rotational motion E_a^{rot} (see the SI for the theoretical treatment and best-fit parameters). All curves follow a BPP behavior, but U at a very low temperature, then its T_1 curve was fitted in the interval 288–373 K. Under a predominant ¹H–¹H dipolar relaxation mechanism, the corresponding correlation time of the dipolar interaction $\tau_C(\text{H})$ can be thought of as the time taken for the molecule to rotate by roughly 1 radian about any axis.⁵⁴ For small rigid molecules, it commonly reflects the molecular reorientational time constant;⁵⁵ for flexible molecules, it has to be rather considered as a combination of molecular reorientation and internal motions of each given segment.^{40,52,56} As observed in Figure 7b and Table S10, the methylene and methyl sites of Ch show very similar $\tau_C(\text{H})$, thus accounting for the whole-molecular motion, with only slight differences coming from the contribution of local motions. Overall, the $\tau_C(\text{H})$ values of Ch aliphatic protons (0.3 ns–25 ps) are shorter than those of U protons (0.7 ns–40 ps). In other words, Ch protons have faster rotational motions than U protons, in line with the qualitative considerations drawn before and in agreement with previous observations on DESs.⁴⁰ Since ⁷Li is a quadrupolar nucleus ($I = 3/2$), the BPP equation for the quadrupolar mechanism has to be applied. Qualitatively, the long $\tau_C(\text{Li})$ values obtained (2–0.2 ns) point toward a slow dynamics for Li, as already observed in several binary mixtures of Li salts and ionic liquids.^{41,57} A physical interpretation of $\tau_C(\text{Li})$ is less intuitive than $\tau_C(\text{H})$, as it reflects the fluctuation of the electric field gradient at the nucleus, which, in turn, depends on the relative positions of the nuclei and its environment and their fluctuations over time.⁵⁸ A possible model, already applied to IL/Li-salt binary mixtures,^{41,57} considers $\tau_C(\text{Li})$ as a descriptor of a single lithium jump from one place to another, with an average one-jump distance defined as $\langle R_{\text{one-flip}} \rangle = \sqrt{6D\tau_C(\text{Li})}$.^{41,57} The estimated average jump distances shown in Figure 7c range between 0.1 and 0.4 nm, thus confirming that very close similarity exists between DES/Li-salt and IL/Li-salt sys-

Table 2. Parameters Obtained From the Linear Fit of the Arrhenius Plot of the Diffusion Data

	278–318 K ^a			323–373 K		
	lnA (m ² s ⁻¹)	E_a^{transl} (kJ mol ⁻¹)	R ²	lnA (m ² s ⁻¹)	E_a^{transl} (kJ mol ⁻¹)	R ²
U	−4.4571	51.7	0.998	−10.7375	34.9	0.998
Ch	−8.4240	42.9	0.999	−11.2336	35.3	0.999
Li	−6.25804	49.4	0.998	−8.90449	42.7	0.995

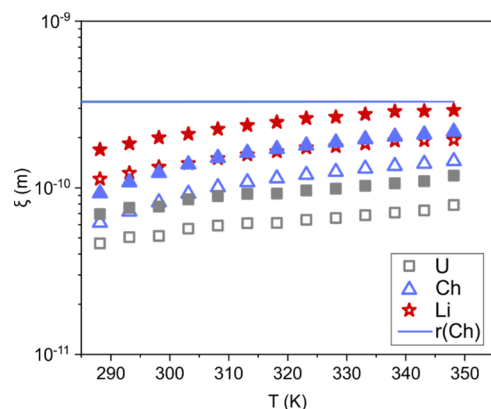
^a D_{Li} at 278 K not available.

Figure 6. Correlation length ξ calculated from the experimental diffusion and viscosity data and plotted as a function of temperature. Full and empty symbols correspond to c equal to 4 or 6, respectively. A reference line for the hard-sphere radius of cholinium (3.29 Å) is also reported.

tems.^{41,57} $\langle R_{\text{one-flip}} \rangle$ at 353 K is approximately 0.3 nm, which is comparable to the first coordination shell of lithium found by MD simulations, suggesting that the lithium solvated by the anion jumps within the solvation sphere. Also, the average one-jump distances obtained from lithium T_1 values nicely match the correlation lengths previously calculated from viscosity and diffusion data for the metal ion (Figure S8), supporting a scenario where lithium ions migrate jumping within the solvation sphere.

For all sites, the apparent activation energy for the rotational motion (averaged over several types of movements) is in the range of 21–26 kJ mol⁻¹, with Li showing a slightly lower value and U at the upper limit (Figure 7d). Overall, the activation energies associated with relaxation data are smaller than those describing translational motions (ca. 20 kJ mol⁻¹ vs 35–50 kJ mol⁻¹), in agreement with behaviors typically observed in similar systems like ionic liquids.^{24,40,41,52,57,59} Noteworthy is the E_a^{rot} estimated for U (25.7 kJ mol⁻¹), which is higher than Ch protons (22.6–24.0 kJ mol⁻¹). This

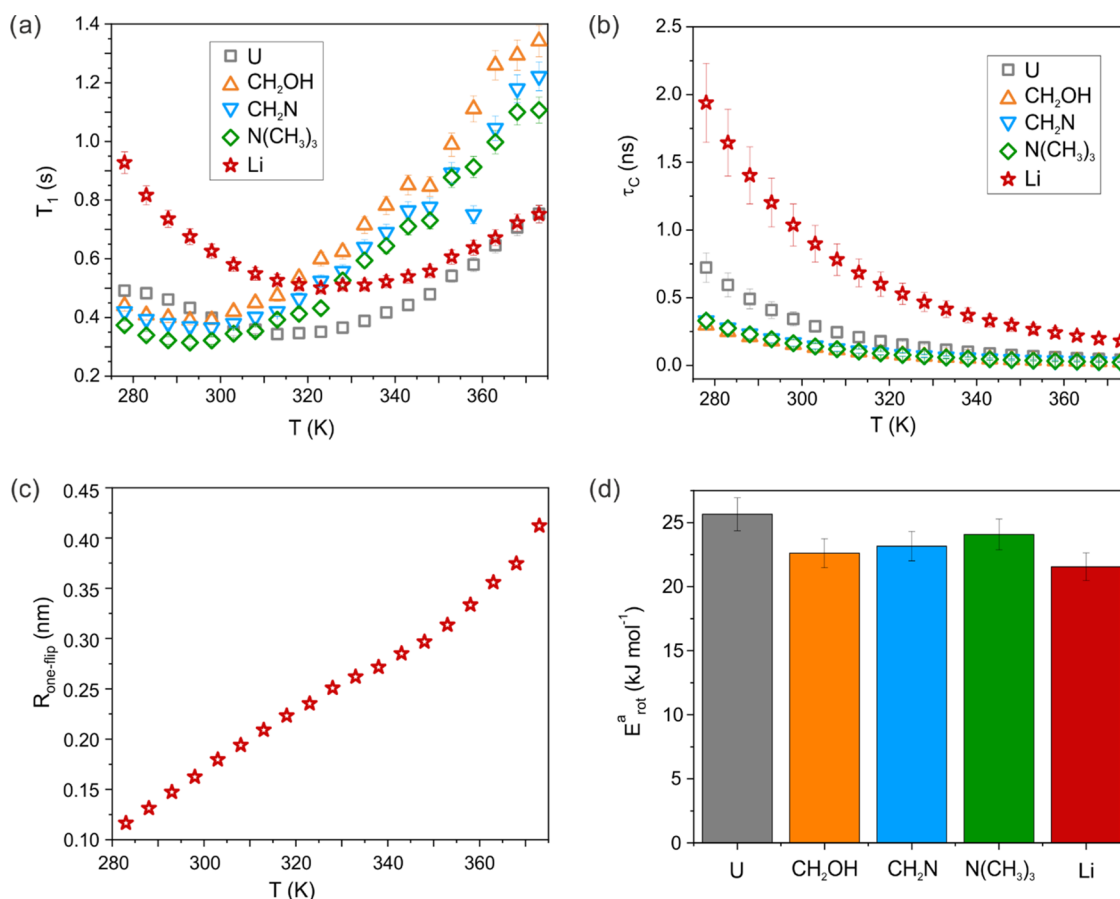


Figure 7. ¹H and ⁷Li (a) T_1 relaxation times and (b) correlation time τ_C , as a function of temperature, (c) average single-jump distance for a lithium ion in the mixture, and (d) the corresponding rotational activation energy E_a^{rot} at the different sites.

Table 3. Experimental and Calculated Reorientational Times (in 10^{-11} s) at 353 K

system	$\tau(\text{N}(\text{CH}_3)_3)$	$\tau(\text{CH}_2\text{N})$	$\tau(\text{CH}_2\text{O})$	$\tau(\text{OH}^{\text{Ch}})$	$\tau(\text{NH}_2)$	$\tau(\text{OH}^{\text{W}})$	$\tau(\text{Li})$
ChCl:U–LiCl–W							
exp	3.6	3.9	3.7		6.8		26.7
calc	4.9	3.3	3.8	8.4	7.6	5.0	
ChCl:U–LiCl							
calc	9.9	6.7	8.4	21.2	18.9		

correlates with the strong and well-known participation of the HBD in the intermolecular network and marks a difference with the structurally related DES composed of choline acetate and urea, where $E_a^{\text{rot}}(\text{U}) < E_a^{\text{rot}}(\text{Ch})$.⁴⁰ A systematic comparison between the two systems with the same composition is needed to draw a definite conclusion, but this observation fits the scenario of more tightly bound U molecules when Cl is the anion with respect to acetate.

The experimental molecular reorientational times were compared to the calculated reorientational times of the X–C bond vectors (Table 3), where X is an atom directly attached to hydrogen. The values are in good agreement even though the simulation does not include internal nuclear and electronic effects. We considered the use of bond vectors to be a reasonable assumption since it takes into account the nearest atomic environment of selected hydrogens. For quadrupolar lithium and chloride ions, a strict computation of the electric field gradient was not addressed and the corresponding correlation times were not calculated. On the other hand, the computational study provides information about the rotation of the OH groups of cholinium and water, which are difficult to obtain experimentally due to poor peak resolution. Indeed, the hydroxyl group of cholinium has the slowest rotation motion among all of the protons in the system because of the important hydrogen-bond interactions with chloride anion (Figure 4a) but still remains faster than strongly coordinated lithium. As expected, water rotation is less hindered in comparison with that of the cholinium cation due to its smaller size.

Isolating Water Contribution. A fully anhydrous system can be prepared in silico to study the influence of water on the structure and dynamics of the ChCl:U–LiCl system. Although at first sight, the local structure of both systems seems identical (Figures 3e–g, S11 and S12 vs 3a–c and 4), careful analysis reveals a decrease in the urea and cholinium contribution in the environment of lithium upon the addition of water. In a water-free system, 6.0 cholinium cations and 7.4 urea molecules are found near the metal ion (at the same characteristic distances) due to enhanced $\text{Li}\cdots\text{O}$ electrostatic interactions. This can be seen in the $\text{Li}\cdots\text{O}_\text{U}$ RDF in Figure 8. Contrasting to this, the lithium chloride association is unaffected, and the remaining anions form H-bonds with H_O and H_U atoms, with coordination numbers reaching 0.74 and 3.40, due to the absence of competition with water. These structural changes are not pronounced, with intermolecular H-bonding patterns being preserved upon water addition, typical of a DES with low water content (<5%).⁶⁰ More complex effects, such as proton exchange between water and cholinium^{39,61} or rearrangements of the interaction network,⁶⁰ can occur when water is intentionally added to the system in quantities much greater than studied in this paper.

The density decreases by a few percentage points when water is added to the DES mixture, as reported in Table 1. Moderate differences between ChCl:U–LiCl and ChCl:U–

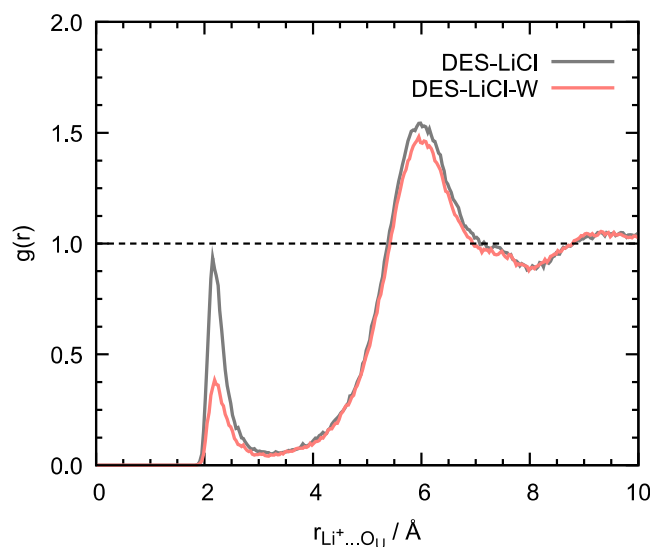


Figure 8. Radial distribution functions of oxygen atoms of urea (O_U) around lithium cation in the ChCl:U–LiCl and ChCl:U–LiCl–W systems.

LiCl–W systems can be noticed in the transport properties. The addition of 3.9% of water increases diffusion coefficients by 2.5–3.0 times, the reorientation is accelerated twice, and viscosity drops down notably even with such a low water content. This behavior is consistent with results on pure DES and DES–water mixtures^{61,62} and is important for many technological applications of our systems, where low viscosity is a desirable property.

CONCLUSIONS

For the first time, a comprehensive picture of the structure and dynamics of the lithium salt LiCl in the archetypal choline-based DES ChCl:U has been outlined using a joint experimental and theoretical approach.

It emerges that lithium cations are strongly coordinated by chloride anions, with the formation of planar triangular LiCl_3^{2-} units. Urea and cholinium are mainly found in the second coordination shell of lithium, indirectly interacting with the cation through the chloride anions. The urea HBD plays indeed a major, temperature-dependent, role in the intermolecular HB network. The strong coordination by chloride anions and the overall involvement of the species in the HB network may pose limitations to the practical use of the system such as electrolytes in LIBs. Nevertheless, DESs are endowed with a huge potential as tunable solvents, which go far beyond ILs. In addition to the various possible combinations of the ionic species, even in the simplest DES system, an extra molecular species is present, and the composition between salt and HBD can be varied. This may be extremely relevant to modifying the structure and transport properties of the electrolyte. Furthermore, mixtures of DESs and controlled

amounts of water may result in better-performing hybrid materials and can be thought of as potential water-in-DES electrolyte systems. Comparison between the DES–LiCl–W and DES–LiCl systems showed that, similarly to pure ChCl:U, the intermolecular structure of the DES electrolyte is preserved upon the addition of small amounts of water, i.e., the presence of the Li salt does not change the structural response of the DES to small amounts of water. As expected, dynamics is strongly affected, as the presence of water leads to a low-viscous fluid, thus enhancing considerably both translational and rotational motions. Contrarily, the strong coordination of lithium by chloride anion is unaffected, with minor differences being observed for the indirect interactions of lithium with urea and cholinium.

The characterization strategy adopted here for a prototype DES electrolyte system can then open new horizons in tailoring the design of functional systems out of the enormous number of possible combinations.

■ ASSOCIATED CONTENT

SI Supporting Information

The Supporting Information is available free of charge at <https://pubs.acs.org/doi/10.1021/acssuschemeng.2c02460>.

Experimental details; NMR supporting data and theoretical toolkit for data analysis; density and viscosity supplementary data; and MD supporting data (PDF)

■ AUTHOR INFORMATION

Corresponding Authors

Maria Enrica Di Pietro – Department of Chemistry, Materials and Chemical Engineering “G. Natta”, Politecnico di Milano, 20133 Milano, Italy; orcid.org/0000-0002-2370-1948; Email: mariaenrica.dipietro@polimi.it

Agilio A. H. Padua – École Normale Supérieure de Lyon and CNRS, Laboratoire de Chimie, 69364 Lyon, France; orcid.org/0000-0002-7641-6526; Email: agilio.padua@ens-lyon.fr

Authors

Kateryna Goloviznina – École Normale Supérieure de Lyon and CNRS, Laboratoire de Chimie, 69364 Lyon, France; Present Address: Sorbonne Université, CNRS, Physico-chimie des Électrolytes et Nanosystèmes Interfaciaux, PHENIX, F-75005 Paris, France; orcid.org/0000-0001-9913-4938

Adriaan van den Bruinhorst – École Normale Supérieure de Lyon and CNRS, Laboratoire de Chimie, 69364 Lyon, France

Giselle de Araujo Lima e Souza – Department of Chemistry, Materials and Chemical Engineering “G. Natta”, Politecnico di Milano, 20133 Milano, Italy

Margarida Costa Gomes – École Normale Supérieure de Lyon and CNRS, Laboratoire de Chimie, 69364 Lyon, France; orcid.org/0000-0001-8637-6057

Andrea Mele – Department of Chemistry, Materials and Chemical Engineering “G. Natta”, Politecnico di Milano, 20133 Milano, Italy; CNR-SCITEC Istituto di Scienze e Tecnologie Chimiche, 20133 Milano, Italy; orcid.org/0000-0002-0351-0538

Complete contact information is available at: <https://pubs.acs.org/doi/10.1021/acssuschemeng.2c02460>

Author Contributions

[†]M.E.D.P. and K.G. authors contributed equally. The manuscript was written through contributions of all authors. All authors have given approval to the final version of the manuscript.

Funding

IDEX-LYON (Programme Investissements d’Avenir ANR-16-IDEX-0005).

Notes

The authors declare no competing financial interest.

■ ACKNOWLEDGMENTS

MD simulations were performed on the computer clusters of the GENCI-IDRIS (Grant 2020-A0090800609) and the Pôle Scientifique de Modélisation Numérique (PSMN) at ENS de Lyon. The authors thank the Regione Lombardia and ENEA for the grant for G.A.L.S. Ph.D. programme.

■ REFERENCES

- (1) Armand, M.; Axmann, P.; Bresser, D.; Copley, M.; Edström, K.; Ekberg, C.; Guyomard, D.; Lestriez, B.; Novák, P.; Petranikova, M.; et al. Lithium-Ion Batteries – Current State of the Art and Anticipated Developments. *J. Power Sources* **2020**, 479, No. 228708.
- (2) Hansen, B. B.; Spittle, S.; Chen, B.; Poe, D.; Zhang, Y.; Klein, J. M.; Horton, A.; Adhikari, L.; Zelovich, T.; Doherty, B. W.; et al. Deep Eutectic Solvents: A Review of Fundamentals and Applications. *Chem. Rev.* **2021**, 121, 1232–1285.
- (3) Jaumaux, P.; Wu, J.; Shanmukaraj, D.; Wang, Y.; Zhou, D.; Sun, B.; Kang, F.; Li, B.; Armand, M.; Wang, G. Non-Flammable Liquid and Quasi-Solid Electrolytes toward Highly-Safe Alkali Metal-Based Batteries. *Adv. Funct. Mater.* **2021**, 31, No. 2008644.
- (4) Watanabe, M.; Thomas, M. L.; Zhang, S.; Ueno, K.; Yasuda, T.; Dokko, K. Application of Ionic Liquids to Energy Storage and Conversion Materials and Devices. *Chem. Rev.* **2017**, 117, 7190–7239.
- (5) Di Pietro, M. E.; Mele, A. Deep Eutectics and Analogues as Electrolytes in Batteries. *J. Mol. Liq.* **2021**, 338, No. 116597.
- (6) Martins, M. A. R.; Pinho, S. P.; Coutinho, J. A. P. Insights into the Nature of Eutectic and Deep Eutectic Mixtures. *J. Solution Chem.* **2019**, 48, 962–982.
- (7) Cruz, H.; Jordão, N.; Branco, L. C. Deep Eutectic Solvents (DESS) as Low-Cost and Green Electrolytes for Electrochromic Devices. *Green Chem.* **2017**, 19, 1653–1658.
- (8) Dhingra, D.; Bhawna, B.; Pandey, A.; Pandey, S. Pyrene Fluorescence to Probe a Lithium Chloride-Added (Choline Chloride + Urea) Deep Eutectic Solvent. *J. Phys. Chem. B* **2019**, 123, 3103–3111.
- (9) Dhingra, D.; Pandey, S. Effect of Lithium Chloride on the Density and Dynamic Viscosity of Choline Chloride/Urea Deep Eutectic Solvent in the Temperature Range (303.15–358.15) K. *J. Chem. Thermodyn.* **2019**, 130, 166–172.
- (10) Barik, S.; Chakraborty, M.; Sarkar, M. How Does Addition of Lithium Salt Influence the Structure and Dynamics of Choline Chloride-Based Deep Eutectic Solvents? *J. Phys. Chem. B* **2020**, 124, 2864–2878.
- (11) Millia, L.; Dall’Asta, V.; Ferrara, C.; Berbenni, V.; Quartarone, E.; Perna, F. M.; Capriati, V.; Mustarelli, P. Bio-Inspired Choline Chloride-Based Deep Eutectic Solvents as Electrolytes for Lithium-Ion Batteries. *Solid State Ionics* **2018**, 323, 44–48.
- (12) Goloviznina, K.; Canongia Lopes, J. N.; Costa Gomes, M.; Pádua, A. A. H. Transferable, Polarizable Force Field for Ionic Liquids. *J. Chem. Theory Comput.* **2019**, 15, S858–S871.
- (13) Goloviznina, K.; Gong, Z.; Costa Gomes, M. F.; Pádua, A. A. H. Extension of the CL&Pol Polarizable Force Field to Electrolytes, Protic Ionic Liquids, and Deep Eutectic Solvents. *J. Chem. Theory Comput.* **2021**, 17, 1606–1617.

- (14) Chen, Y.; Yu, D.; Chen, W.; Fu, L.; Mu, T. Water Absorption by Deep Eutectic Solvents. *Phys. Chem. Chem. Phys.* **2019**, *21*, 2601–2610.
- (15) Hammond, O. S.; Bowron, D. T.; Edler, K. J. The Effect of Water upon Deep Eutectic Solvent Nanostructure: An Unusual Transition from Ionic Mixture to Aqueous Solution. *Angew. Chem., Int. Ed.* **2017**, *56*, 9782–9785.
- (16) Gabl, S.; Steinhauser, O.; Weingärtner, H. From Short-Range to Long-Range Intermolecular NOEs in Ionic Liquids: Frequency Does Matter. *Angew. Chem., Int. Ed.* **2013**, *52*, 9242–9246.
- (17) Castiglione, F.; Appetecchi, G. B.; Passerini, S.; Panzeri, W.; Indelicato, S.; Mele, A. Multiple Points of View of Heteronuclear NOE: Long Range vs Short Range Contacts in Pyrrolidinium Based Ionic Liquids in the Presence of Li Salts. *J. Mol. Liq.* **2015**, *210*, 215–222.
- (18) Honegger, P.; Di Pietro, M. E.; Castiglione, F.; Vaccarini, C.; Quant, A.; Steinhauser, O.; Schröder, C.; Mele, A. The Intermolecular NOE Depends on Isotope Selection: Short Range vs Long Range Behavior. *J. Phys. Chem. Lett.* **2021**, *12*, 8658–8663.
- (19) Lingscheid, Y.; Paul, M.; Bröhl, A.; Neudörfl, J.; Giernoth, R. Determination of Inter-Ionic and Intra-Ionic Interactions in a Monofluorinated Imidazolium Ionic Liquid by a Combination of X-Ray Crystallography and NOE NMR Spectroscopy. *Magn. Reson. Chem.* **2018**, *56*, 80–85.
- (20) Lingscheid, Y.; Arenz, S.; Giernoth, R. Heteronuclear NOE Spectroscopy of Ionic Liquids. *ChemPhysChem* **2012**, *13*, 261–266.
- (21) Bolimowska, E.; Castiglione, F.; Devemy, J.; Rouault, H.; Mele, A.; Pádua, A.A.H.; Santini, C. C. Investigation of Li⁺ Cation Coordination and Transportation, by Molecular Modeling and NMR Studies, in a LiNTf₂-Doped Ionic Liquid-Vinylene Carbonate Mixture. *J. Phys. Chem. B* **2018**, *122*, 8560–8569.
- (22) Tsuzuki, S.; Shinoda, W.; Matsugami, M.; Umebayashi, Y.; Ueno, K.; Mandai, T.; Seki, S.; Dokko, K.; Watanabe, M. Structures of [Li(Glyme)]⁺ Complexes and Their Interactions with Anions in Equimolar Mixtures of Glymes and Li[TFSA]: Analysis by Molecular Dynamics Simulations. *Phys. Chem. Chem. Phys.* **2015**, *17*, 126–129.
- (23) Saito, S.; Watanabe, H.; Ueno, K.; Mandai, T.; Seki, S.; Tsuzuki, S.; Kameda, Y.; Dokko, K.; Watanabe, M.; Umebayashi, Y. Li⁺ Local Structure in Hydrofluoroether Diluted Li-Glyme Solvate Ionic Liquid. *J. Phys. Chem. B* **2016**, *120*, 3378–3387.
- (24) Nürnberg, P.; Lozinskaya, E. I.; Shaplov, A. S.; Schönhoff, M. Li Coordination of a Novel Asymmetric Anion in Ionic Liquid-in-Li Salt Electrolytes. *J. Phys. Chem. B* **2020**, *124*, 861–870.
- (25) Huang, Q.; Lourenço, T. C.; Costa, L. T.; Zhang, Y.; Maginn, E. J.; Gurkan, B. Solvation Structure and Dynamics of Li⁺ in Ternary Ionic Liquid–Lithium Salt Electrolytes. *J. Phys. Chem. B* **2019**, *123*, S16–S27.
- (26) Fujii, K.; Hamano, H.; Doi, H.; Song, X.; Tsuzuki, S.; Hayamizu, K.; Seki, S.; Kameda, Y.; Dokko, K.; Watanabe, M.; Umebayashi, Y. Unusual Li⁺ Ion Solvation Structure in Bis-(Fluorosulfonyl)Amide Based Ionic Liquid. *J. Phys. Chem. C* **2013**, *117*, 19314–19324.
- (27) Méndez-Morales, T.; Carrete, J.; Bouzón-Capelo, S.; Pérez-Rodríguez, M.; Cabeza, O.; Gallego, L. J.; Varela, L. M. MD Simulations of the Formation of Stable Clusters in Mixtures of Alkaline Salts and Imidazolium-Based Ionic Liquids. *J. Phys. Chem. B* **2013**, *117*, 3207–3220.
- (28) Méndez-Morales, T.; Carrete, J.; Rodríguez, J. R.; Cabeza, Ó.; Gallego, L. J.; Russina, O.; Varela, L. M. Nanostructure of Mixtures of Protic Ionic Liquids and Lithium Salts: Effect of Alkyl Chain Length. *Phys. Chem. Chem. Phys.* **2015**, *17*, 5298–5307.
- (29) Ray, P.; Vogl, T.; Balducci, A.; Kirchner, B. Structural Investigations on Lithium-Doped Protic and Aprotic Ionic Liquids. *J. Phys. Chem. B* **2017**, *121*, S279–S292.
- (30) Lassègues, J.-C.; Grondin, J.; Talaga, D. Lithium Solvation in Bis-(Trifluoromethanesulfonyl)Imide-Based Ionic Liquids. *Phys. Chem. Chem. Phys.* **2006**, *8*, S629–S632.
- (31) Duluard, S.; Grondin, J.; Bruneel, J. L.; Pianet, I.; Grélard, A.; Campet, G.; Delville, M. H.; Lassègues, J. C. Lithium Solvation and Diffusion in the 1-Butyl-3-Methylimidazolium Bis-(Trifluoromethanesulfonyl)Imide Ionic Liquid. *J. Raman Spectrosc.* **2008**, *39*, 627–632.
- (32) Vogl, T.; Goodrich, P.; Jacquemin, J.; Passerini, S.; Balducci, A. The Influence of Cation Structure on the Chemical-Physical Properties of Protic Ionic Liquids. *J. Phys. Chem. C* **2016**, *120*, 8525–8533.
- (33) Umebayashi, Y.; Hamano, H.; Seki, S.; Minofar, B.; Fujii, K.; Hayamizu, K.; Tsuzuki, S.; Kameda, Y.; Kohara, S.; Watanabe, M. Liquid Structure of and Li⁺ Ion Solvation in Bis-(Trifluoromethanesulfonyl)Amide Based Ionic Liquids Composed of 1-Ethyl-3-Methylimidazolium and N-Methyl-N-Propylpyrrolidinium Cations. *J. Phys. Chem. B* **2011**, *115*, 12179–12191.
- (34) Ashworth, C. R.; Matthews, R. P.; Welton, T.; Hunt, P. A. Doubly Ionic Hydrogen Bond Interactions within the Choline Chloride – Urea Deep Eutectic Solvent. *Phys. Chem. Chem. Phys.* **2016**, *18*, 18145–18160.
- (35) Fetisov, E. O.; Harwood, D. B.; Kuo, I.-F.W.; Warrag, S. E. E.; Kroon, M. C.; Peters, C. J.; Siepmann, J. I. First-Principles Molecular Dynamics Study of a Deep Eutectic Solvent: Choline Chloride/Urea and Its Mixture with Water. *J. Phys. Chem. B* **2018**, *122*, 1245–1254.
- (36) Sapir, L.; Harries, D. Restructuring a Deep Eutectic Solvent by Water: The Nanostructure of Hydrated Choline Chloride/Urea. *J. Chem. Theory Comput.* **2020**, *16*, 3335–3342.
- (37) Triolo, A.; Lo Celso, F.; Brehm, M.; Di Lisio, V.; Russina, O. Liquid Structure of a Choline Chloride-Water Natural Deep Eutectic Solvent: A Molecular Dynamics Characterization. *J. Mol. Liq.* **2021**, *331*, No. 115750.
- (38) D'Agostino, C.; Harris, R. C.; Abbott, A. P.; Gladden, L. F.; Mantle, M. D. Molecular Motion and Ion Diffusion in Choline Chloride Based Deep Eutectic Solvents Studied by 1H Pulsed Field Gradient NMR Spectroscopy. *Phys. Chem. Chem. Phys.* **2011**, *13*, 21383–21391.
- (39) D'Agostino, C.; Gladden, L. F.; Mantle, M. D.; Abbott, A. P.; Ahmed, E. I.; Al-Murshedi, A. Y. M.; Harris, R. C. Molecular and Ionic Diffusion in Aqueous-Deep Eutectic Solvent Mixtures: Probing Inter-Molecular Interactions Using PFG NMR. *Phys. Chem. Chem. Phys.* **2015**, *17*, 15297–15304.
- (40) Triolo, A.; Di Pietro, M. E.; Mele, A.; Lo Celso, F.; Brehm, M.; Di Lisio, V.; Martinelli, A.; Chater, P.; Russina, O. Liquid Structure and Dynamics in the Choline Acetate:Urea 1:2 Deep Eutectic Solvent. *J. Chem. Phys.* **2021**, *154*, No. 244501.
- (41) Hayamizu, K.; Tsuzuki, S.; Seki, S.; Fujii, K.; Suenaga, M.; Umebayashi, Y. Studies on the Translational and Rotational Motions of Ionic Liquids Composed of N-Methyl-N-Propyl-Pyrrolidinium (P13) Cation and Bis-(Trifluoromethanesulfonyl)Amide and Bis-(Fluorosulfonyl)Amide Anions and Their Binary Systems Including Lithium Salts. *J. Chem. Phys.* **2010**, *133*, No. 194505.
- (42) Castiglione, F.; Ragg, E.; Mele, A.; Appetecchi, G. B.; Montanino, M.; Passerini, S. Molecular Environment and Enhanced Diffusivity of Li⁺ Ions in Lithium-Salt-Doped Ionic Liquid Electrolytes. *J. Phys. Chem. Lett.* **2011**, *2*, 153–157.
- (43) Litovitz, T. A. Temperature Dependence of the Viscosity of Associated Liquids. *J. Chem. Phys.* **1952**, *20*, 1088–1089.
- (44) Rauber, D.; Philippi, F.; Zapp, J.; Kickelbick, G.; Natter, H.; Hempelmann, R. Transport Properties of Protic and Aprotic Guanidinium Ionic Liquids. *RSC Adv.* **2018**, *8*, 41639–41650.
- (45) Duarte, A. R. C.; Ferreira, A. S. D.; Barreiros, S.; Cabrita, E.; Reis, R. L.; Paiva, A. A Comparison between Pure Active Pharmaceutical Ingredients and Therapeutic Deep Eutectic Solvents: Solubility and Permeability Studies. *Eur. J. Pharm. Biopharm.* **2017**, *114*, 296–304.
- (46) Taylor, A. W.; Licence, P.; Abbott, A. P. Non-Classical Diffusion in Ionic Liquids. *Phys. Chem. Chem. Phys.* **2011**, *13*, 10147–10154.
- (47) Fryars, S.; Limanton, E.; Gau, F.; Paquin, L.; Lagrost, C.; Hapiot, P. Diffusion of Redox Active Molecules in Deep Eutectic Solvents. *J. Electroanal. Chem.* **2018**, *819*, 214–219.

- (48) Kholodenko, A. L.; Douglas, J. F. Generalized Stokes-Einstein Equation for Spherical Particle Suspensions. *Phys. Rev. E* **1995**, *51*, 1081–1090.
- (49) Abbott, A. P.; Harris, R. C.; Ryder, K. S.; D'Agostino, C.; Gladden, L. F.; Mantle, M. D. Glycerol Eutectics as Sustainable Solvent Systems. *Green Chem.* **2011**, *13*, 82–90.
- (50) Harris, K. R. Scaling the Transport Properties of Molecular and Ionic Liquids. *J. Mol. Liq.* **2016**, *222*, 520–534.
- (51) Bloembergen, N.; Purcell, E. M.; Pound, R. V. Relaxation Effects in Nuclear Magnetic Resonance Absorption. *Phys. Rev.* **1948**, *73*, 679–712.
- (52) Di Pietro, M. E.; Castiglione, F.; Mele, A. Polar / Apolar Domains' Dynamics in Alkylimidazolium Ionic Liquids Unveiled by the Dual Receiver NMR ^1H and ^{19}F Relaxation Experiment. *J. Mol. Liq.* **2021**, *322*, No. 114567.
- (53) Mohammadi, M.; Benders, S.; Jerschow, A. Nuclear Magnetic Resonance Spin-Lattice Relaxation of Lithium Ions in Aqueous Solution by NMR and Molecular Dynamics. *J. Chem. Phys.* **2020**, *153*, No. 184502.
- (54) Neuhaus, D.; Williamson, M. *The Nuclear Overhauser Effect in Structural and Conformational Analysis*, 2nd ed.; Wiley: New York, 2000.
- (55) Hayamizu, K.; Tsuzuki, S.; Seki, S.; Umebayashi, Y. Multinuclear NMR Studies on Translational and Rotational Motion for Two Ionic Liquids Composed of BF_4 Anion. *J. Phys. Chem. B* **2012**, *116*, 11284–11291.
- (56) Alam, T. M.; Dreyer, D. R.; Bielwaski, C. W.; Ruoff, R. S. Measuring Molecular Dynamics and Activation Energies for Quaternary Acyclic Ammonium and Cyclic Pyrrolidinium Ionic Liquids Using ^{14}N NMR Spectroscopy. *J. Phys. Chem. A* **2011**, *115*, 4307–4316.
- (57) Hayamizu, K.; Tsuzuki, S.; Seki, S.; Umebayashi, Y. Nuclear magnetic resonance studies on the rotational and translational motions of ionic liquids composed of 1-ethyl-3-methylimidazolium cation and bis (trifluoromethanesulfonyl) amide and bis (fluorosulfonyl) amide anions and their binary systems including lithium salts. *J. Chem. Phys.* **2011**, *135*, No. 084505.
- (58) Carof, A.; Salanne, M.; Charpentier, T.; Rotenberg, B. Collective Water Dynamics in the First Solvation Shell Drive the NMR Relaxation of Aqueous Quadrupolar Cations. *J. Chem. Phys.* **2016**, *145*, No. 124508.
- (59) Di Pietro, M. E.; Castiglione, F.; Mele, A. Anions as Dynamic Probes for Ionic Liquid Mixtures. *J. Phys. Chem. B* **2020**, *124*, 2879–2891.
- (60) Shah, D.; Mjalli, F. S. Effect of Water on the Thermo-Physical Properties of Reline: An Experimental and Molecular Simulation Based Approach. *Phys. Chem. Chem. Phys.* **2014**, *16*, 23900–23907.
- (61) Posada, E.; López-Salas, N.; Jiménez Riobó, R. J.; Ferrer, M. L.; Gutiérrez, M. C.; Del Monte, F. Reline Aqueous Solutions Behaving as Liquid Mixtures of H-Bonded Co-Solvents: Microphase Segregation and Formation of Co-Continuous Structures as Indicated by Brillouin And ^1H NMR Spectroscopies. *Phys. Chem. Chem. Phys.* **2017**, *19*, 17103–17110.
- (62) Agieienko, V.; Buchner, R. Densities, Viscosities, and Electrical Conductivities of Pure Anhydrous Reline and Its Mixtures with Water in the Temperature Range (293.15 to 338.15) K. *J. Chem. Eng. Data* **2019**, *64*, 4763–4774.

Recommended by ACS

Dynamic Water Promotes Lithium-Ion Transport in Superconcentrated and Eutectic Aqueous Electrolytes

Jungyu Kim, Minhaeng Cho, *et al.*

DECEMBER 10, 2021
ACS ENERGY LETTERS

READ 

Understanding Solvation Behavior of the Saturated Electrolytes with Small/Wide-Angle X-ray Scattering and Raman Spectroscopy

Kun Qian, Tao Li, *et al.*

NOVEMBER 11, 2021
ENERGY & FUELS

READ 

Molecular Structure, Chemical Exchange, and Conductivity Mechanism of High Concentration LiTFSI Electrolytes

Susith R. Galle Kankanamge and Daniel G. Kuroda

FEBRUARY 18, 2020
THE JOURNAL OF PHYSICAL CHEMISTRY B

READ 

Solvation Structure around Li^+ Ions in Organic Carbonate Electrolytes: Spacer-Free Thin Cell IR Spectroscopy

Chaiho Lim, Minhaeng Cho, *et al.*

SEPTEMBER 07, 2021
ANALYTICAL CHEMISTRY

READ 

Get More Suggestions >